

Supplementary Information

Ultrafast Flow Chemistry for the Acid-Catalyzed Conversion of Fructose

Pierre Desir^{a,b}, Basudeb Saha^b, and Dionisios G. Vlachos^{a,b,*}

^a*Department of Chemical and Biomolecular Engineering, University of Delaware, 150 Academy Street, Newark, Delaware 19716, United States*

^b*Catalysis Center for Energy Innovation, 221 Academy Street, Newark, Delaware 19716, United States*

*Corresponding author

Email address: vlachos@udel.edu (D.G. Vlachos)

Publications of Fructose Dehydration to HMF

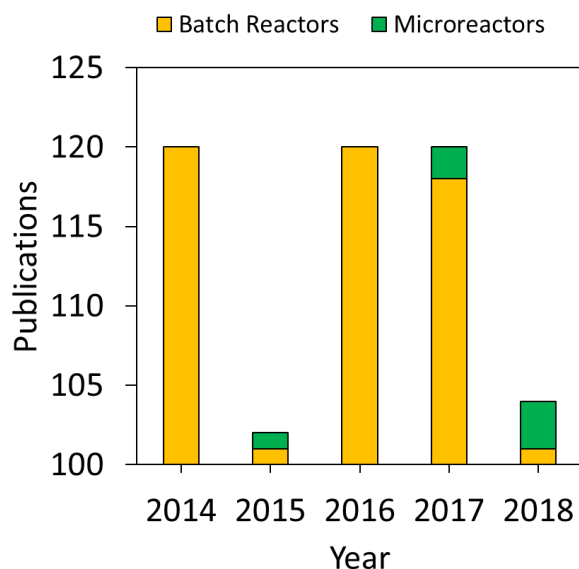


Figure S1: Number of publications on HMF production from fructose in batch reactors and microreactors. Accessed on 10/15/2018. Web of Science search keywords: biomass, fructose, HMF, microreactor.

Temperature Uniformity

The temperature uniformity in the microreactor is evaluated by measuring the inlet and outlet temperatures at short residence times. Since the fructose feed enters the micromixer close to room temperature while the catalyst feed is preheated to the reaction temperature prior to mixing, an

appropriate flow rate ratio between the two feeds is determined to maintain the inlet mixing temperature relatively close to the furnace/reaction temperature. Figure S2 shows the effects of various volumetric flow rate ratios (HCl/fructose (v/v)) on the mixed feeds' (pure deionized water is used for both feeds for the temperature measurements) inlet and outlet temperatures for the shortest residence time (1 s) and for the highest reaction temperature (200 °C) considered herein. The inlet temperature increases with increasing volumetric flow rate ratio of the preheated catalyst to the fructose feeds. For an HCl/fructose (v/v) = 25, the inlet temperature is 198.2 °C when the furnace temperature is set at 200 °C.

The microchannel length required for the inlet mixture to reach the furnace temperature was determined experimentally. Figure S3 shows the temperature at various channel lengths from the mixer, for a total flow rate (Q_{total}) of 10.4 mL/min, which corresponds to a residence time of 1 s in the 1 m long microchannel. The temperature at all locations reaches the furnace temperature within a standard deviation of ± 0.1 °C. Thus, a coiled channel length of <5 cm is sufficient to bring the mixed feed to the furnace temperature. Given that this length is <5% of the actual microchannel length, temperature uniformity is achieved shortly after the entrance.

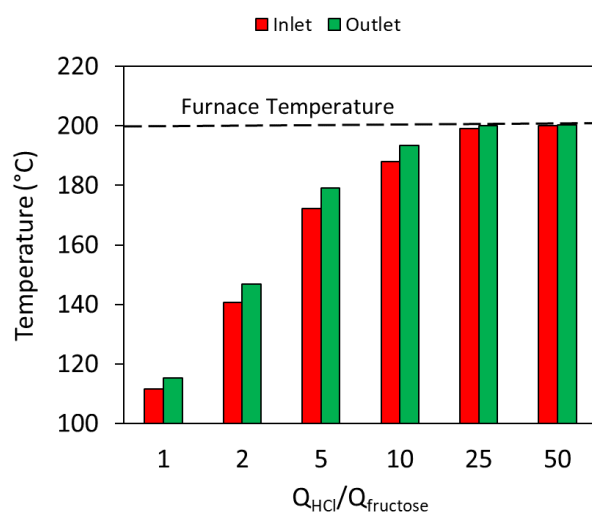


Figure S2: Measured inlet and outlet temperature of the coiled microreactor as a function of the ratio between the volumetric flow rate of the HCl feed (Q_{HCl}) and the volumetric flow rate of fructose feed ($Q_{Fructose}$) pumps using deionized water as the working fluid. Conditions: furnace temperature = 200 °C, coiled microchannel length = 1 m, residence time = 1 s, Q_{total} = 10.4 mL/min.

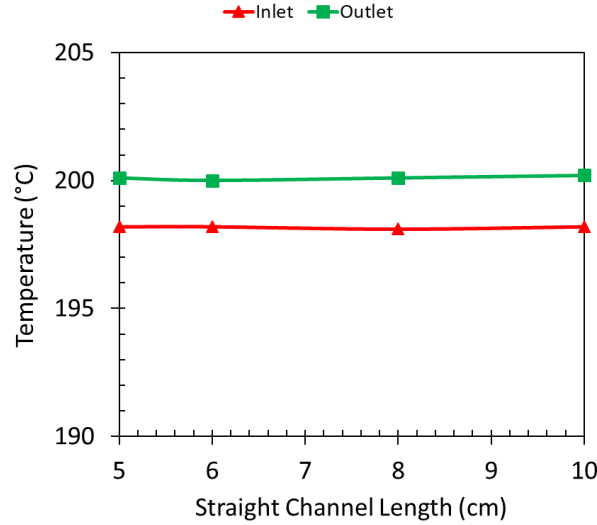


Figure S3: Measured inlet and outlet temperature of the coiled microreactor as a function of channel length, using deionized water as the working fluid. Conditions: furnace temperature = 200 °C, $Q_{total} = 10.4$ mL/min, $Q_{HCl}/Q_{Fructose} = 25$.

Microreactor Inlet Temperature Calculation

The microreactor inlet temperature, T_{in} , is estimated by doing a mass and energy balance over the T-micromixer (control volume) under adiabatic conditions since the heating rate of the oven is unknown. Scheme S1 shows an illustration of the control volume considered for the calculations. The fructose feed mass flow rate, volumetric flow rate, and temperature are \dot{m}_1 , Q_1 , and T_1 , respectively. The HCl feed mass flow rate, volumetric flow rate, and temperature are \dot{m}_2 , Q_2 , and T_2 , respectively. The microreactor inlet feed mass flow rate, volumetric flow rate, and temperature are \dot{m}_{in} , Q_{in} , and T_{in} , respectively. The feeds are assumed to have the properties of pure water. Considering the aqueous solution in the T-micromixer as the system, we assume that the system is running as steady state with constant density, ρ , and specific heat capacity, C_p . The balances can be written as follows:

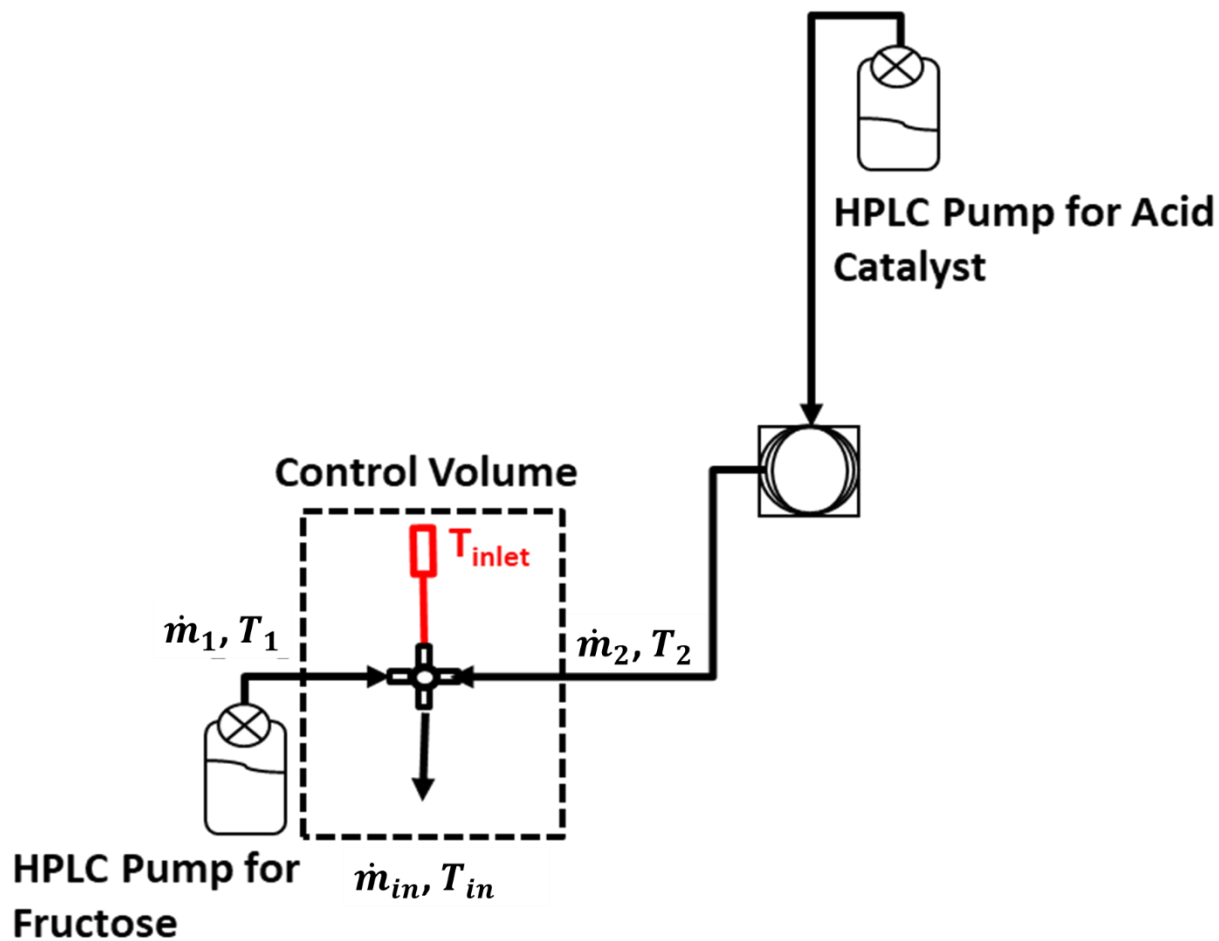
Mass balance:

$$\dot{m}_{in} = \dot{m}_1 + \dot{m}_2 \quad (S1)$$

Energy balance:

$$\dot{m}_{in}C_p(T_{in} - T_{ref}) = \dot{m}_1C_p(T_1 - T_{ref}) + \dot{m}_2C_p(T_2 - T_{ref}) \quad (S2)$$

where T_{ref} is the reference temperature of 25 °C.



Scheme S1: Schematic of the control volume of the microreactor used to estimate the inlet temperature upon mixing under adiabatic conditions.

The subsequent equation calculates the inlet temperature to the microreactor:

$$T_{in} = \left(\frac{Q_1}{Q_1 + Q_2} \right) T_1 + \left(\frac{Q_2}{Q_1 + Q_2} \right) T_2 \quad (S3)$$

or

$$T_{in} = \left(\frac{1}{1 + R} \right) T_1 + \left(\frac{R}{1 + R} \right) T_2 \quad (S4)$$

where $R = \frac{Q_2}{Q_1} = 25$ is the volumetric flow rate ratio between the acid and fructose feeds. Table S1 summarizes the values of the parameters for the feeds at a residence time of 1 s and for the highest temperature considered in the kinetic study:

Table S1. Conditions for the calculation of the inlet temperature upon mixing in the T-shaped micromixer under adiabatic conditions, for a residence time of 1 s and R = 25.

Feed	Density (kg/m ³)	Specific heat capacity (kJ/kg-K)	Volumetric flow rate (mL/min)	Mass flow rate (kg/s)	Temperature (°C)
1 ^a	1000	4.18	0.4	6.67 x 10 ⁻⁶	20
2 ^a	1000	4.18	10	1.67 x 10 ⁻⁴	200

^aThe fructose feed and the HCl feed are labeled as feeds 1 and 2, respectively, since the calculations and the actual measurements were conducted with pure deionized water in each feed.

It follows that $T_{in} = 193.1$ °C. The measured inlet temperature (198.2 °C) exceeds the estimated inlet temperature (193.1 °C) found by a simple mass and energy balance over the T-shaped micromixer under adiabatic conditions. This deviation is reasonable given the assumptions of constant fluid properties and adiabaticity.

Microreactor Outlet Temperature Calculation

The microreactor outlet temperature can be estimated by modeling the heat transfer to the microchannel through three different mechanisms:

- 1) Convective heat transfer from the hot air in the furnace to the channel outer wall.
- 2) Conductive heat transfer through the channel wall.
- 3) Convective heat transfer from the channel inner wall to the aqueous solution.

The heating rate of the microchannel, q , is given by the equation:

$$q = \bar{U}A(T_f - T_m) \quad (S5)$$

where A is the surface area of heat transfer, T_f is the furnace or hot air temperature, T_m is the average temperature of the aqueous solution along the channel cross-section, and \bar{U} is overall heat transfer coefficient, which is defined in terms of the sum of the heat transfer resistances:

$$\frac{1}{\bar{U}} = R_{conv,water} + R_{cond,channel} + R_{conv,air} \quad (S6)$$

where $R_{conv,water}$, $R_{cond,channel}$, and $R_{conv,air}$ are respectively the heat transfer resistances by convection from the water flow, by conduction through the channel wall, and by convection from the hot air circulating in the furnace, respectively. The overall heat transfer coefficient can also be written as:

$$\frac{1}{\bar{U}} = \frac{d_i}{d_o h_{water}} + \frac{d_o}{k_{channel}} \ln\left(\frac{d_o}{d_i}\right) + \frac{1}{h_{air}} \quad (S7)$$

where d_i and d_o are respectively the inner and outer diameter of the microchannel, h_{air} is the convective heat transfer coefficient of hot air at low speed obtained from reported literature values,

and h_{water} is the heat transfer coefficient of water, which is defined in terms of the Nusselt number:

$$Nu = \frac{h_{water}d_i}{k_{water}} \quad (S8)$$

where Nu is the Nusselt number for the coiled microchannel and k_{water} is the thermal conductivity of water. In determining the overall heat transfer coefficient, we also consider the empirical correlations to evaluate Nu , depending on the fact that we have fully developed or developing hydrodynamic and thermal conditions, in order to take into account the entrance effects on the heat transfer. Thereon, we calculate the hydrodynamic entrance length, L_H , and the thermal entrance length, L_T , based on the following equations:

$$L_H = 0.05Red_i \quad (S9)$$

$$L_T = 0.033RePrd_i \quad (S10)$$

where Pr is the Prandtl number defined in terms of the kinematic viscosity, ν , and the thermal diffusivity, α :

$$Pr = \frac{\nu}{\alpha} \quad (S11)$$

The entrance lengths were estimated for the conditions reported in Table S2, for the highest total flow rate and highest temperature considered for the kinetic study. From the calculations, $L_H = 0.56 \text{ cm}$ and $L_T = 5.6 \text{ cm}$. Under these conditions, a fully developed velocity profile is assumed. The Nusselt number for the coiled microchannel is then evaluated. For a fully developed temperature profile, the Nusselt number is given by¹:

$$Nu = \left[\left(3.657 + \frac{4.364}{x_1} \right)^3 + 1.158 \left(\frac{De}{x_2} \right)^{3/2} \right]^{1/3} \quad (S12)$$

$$x_1 = \left(1 + \frac{957}{De^2Pr} \right)^2 \quad (S13)$$

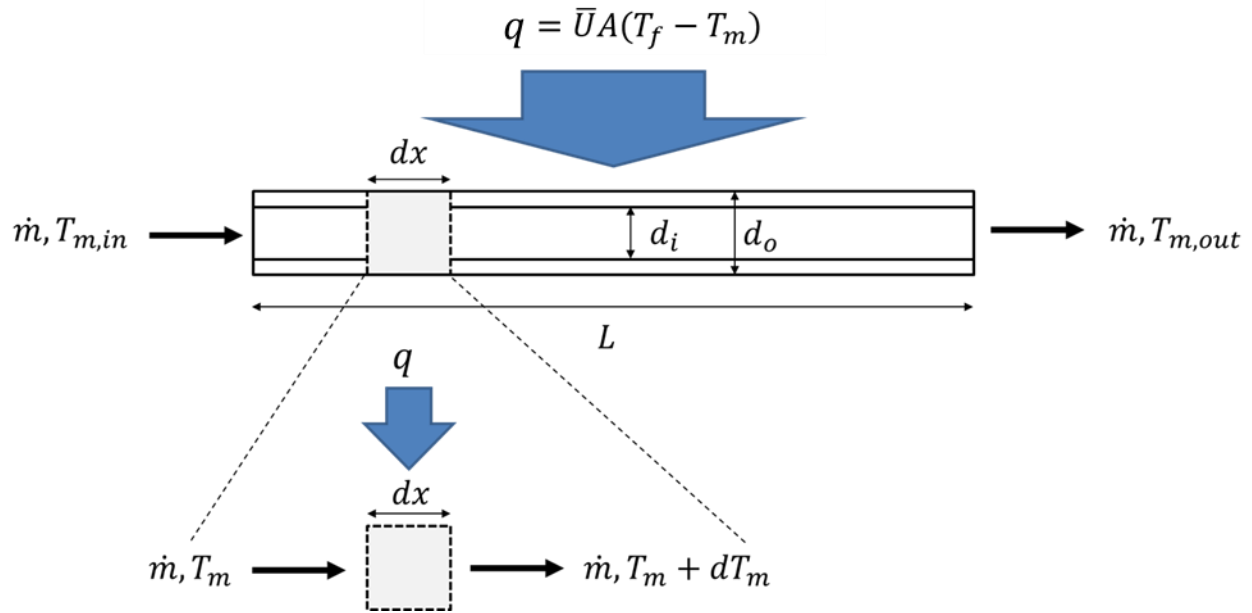
$$x_2 = 1 + \frac{0.477}{Pr} \quad (S14)$$

For a developing temperature profile along the coiled microchannel, the Nusselt number is determined by¹:

$$Nu = \left[\left(4.364 + \frac{4.636}{x_3} \right)^3 + 1.816 \left(\frac{De}{x_4} \right)^{3/2} \right]^{1/3} \quad (S15)$$

$$x_3 = \left(1 + \frac{1342}{De^2 Pr}\right)^2 \quad (S16)$$

$$x_4 = 1 + \frac{1.15}{Pr} \quad (S17)$$



Scheme S2: Schematic representation of the heat transfer to the microchannel inside the furnace.

Table S2. Parameters for the calculation of the microreactor outlet temperature.

\dot{m} (kg/s)	C_p (kJ/kg-K)	d_i (mm)	d_o (mm)	h_{air} (W/m ² -K)	$k_{channel}$ (W/m-K)	T_f (°C)	$T_{m,in}$ (°C)
0.00017	4.18	0.5	1.6	10	0.209	200	20

Scheme S2 shows a schematic of the heat transfer process inside the furnace where the aqueous solution flows through the microchannel of length, L , and constant mass flow rate, \dot{m} , with average inlet temperature, $T_{m,in}$ (inlet temperature measured experimentally), and average outlet temperature, $T_{m,out}$. Considering the energy balance on a differential portion of the microchannel, $T_{m,out}$ can be estimated as a function of the microchannel length:

$$\dot{m}C_p dT_m = \bar{U}\pi d_o(T_f - T_m)dx \quad (S18)$$

$$T_{m,out} = T_f + (T_{m,in} - T_f)e^{\left(\frac{\bar{U}\pi d_o L}{\dot{m}C_p}\right)} \quad (S19)$$

Figure S4 shows the predicted average outlet temperature as a function of the microchannel length. Overall, the heat transfer model estimates that a microchannel length of 4 cm is sufficient to bring the inlet aqueous mixture to the furnace temperature. This value is comparable to the 5 cm of heating length experimentally measured. It should be noted that the heating length upon mixing could not be measured for distances shorter than 5 cm since the geometrical restrictions of the coiled microchannel only allowed for channels with length of at least 5 cm. The temperature variation is by design small and inconsequential to measure. Modeling of heat transfer corroborates with the fact that the temperature variation should be tiny and comparable to our experimental findings. This nearly isothermal condition is in fact what matters rather than having a precise measurement.

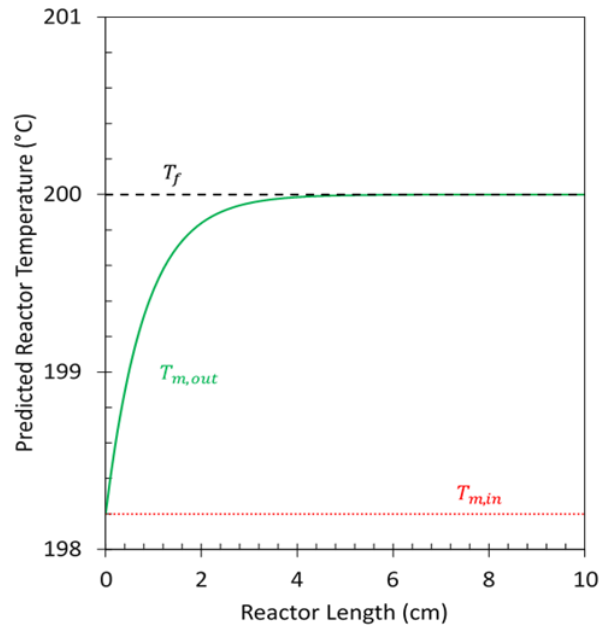


Figure S4: Modeled reactor outlet temperature as a function of reactor length. Conditions: $T_f = 200$ °C, $T_{m,in} = 198.2$ °C, and $Q_{total} = 10.4$ mL/min.

Mixing Characterization

In order to quantify the mixing in the microreactor, the percent mixing was estimated by the following equation:

$$\text{Percent Mixing} = 100\% \times \left(1 - \frac{\sqrt{\frac{\sum_{i=1}^N (I_i - I_i^{\text{Perf,mix}})^2}{N} - \sigma_n^2}}{\sqrt{\frac{\sum_{i=1}^N (I_i^0 - I_i^{\text{Perf,mix}})^2}{N} - \sigma_n^2}} \right) \quad (\text{S20})$$

Here, I_i , $I_i^{\text{Perf,mix}}$, I_i^0 are the intensities of the dye at pixel i , respectively, for (i) the solution flowing through the microchannel at a given cross-section, (ii) the perfectly mixed feed solutions, and (iii) the unmixed dye solution (concentrated sodium fluorescein feed solution). N is the number of pixels at the cross-section and σ_n^2 is the noise in intensity. The intensity is normalized by the maximum intensity in the unmixed case and ranges from 0 to 1.

After estimating the mixing length graphically, the mixing time t_{mixing} is calculated using the cross-sectional area A_c of the microchannel and the total volumetric flow rate Q_{total} .

$$t_{\text{mixing}} = \frac{L_{\text{mixing}} \times A_c}{Q_{\text{total}}} \quad (\text{S21})$$

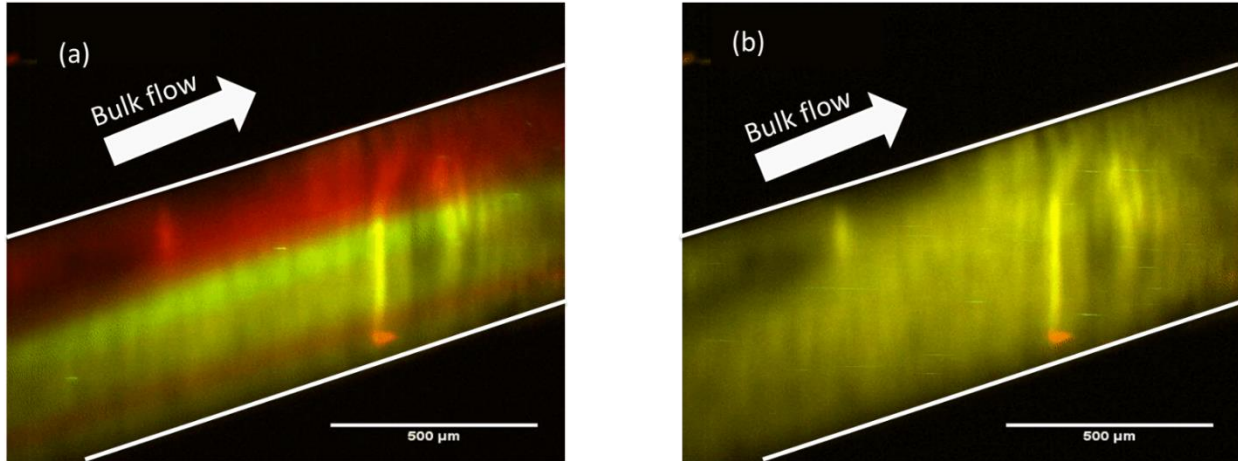


Figure S5: Top view of the first coil of the microreactor obtained by LIF using a high speed confocal microscope and showing the downstream mixing of a feed of sodium fluorescein (green) and a feed of Texas Red dye (red) flowing at a 1:1 flow rate ratio and Q_{total} of 2 mL/min (a) and 10 mL/min (b). Image (a) presents a case of poor mixing from the degree of segregation of the dyes whereas image (b) illustrates a case where complete mixing of the dyes is achieved at that location.

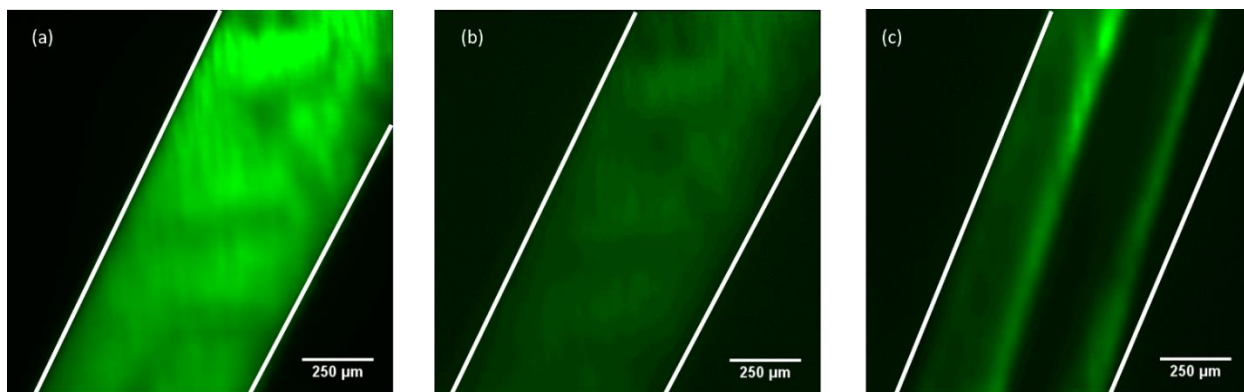


Figure S6: Top view of the fourth coil of the microreactor obtained by LIF using a high speed confocal microscope and showing the flow of an unmixed/250 μM concentrated sodium fluorescein solution (a), a sodium fluorescein solution perfectly pre-mixed/mixed before pumping with deionized water at a 25:1 volume ratio between the fluorescein and the water streams (b), and a sodium fluorescein feed mixing with a feed of deionized water (c) at a 25:1 flow rate ratio between the fluorescein and the water feeds. Conditions: $Q_{total} = 2$ mL/min.

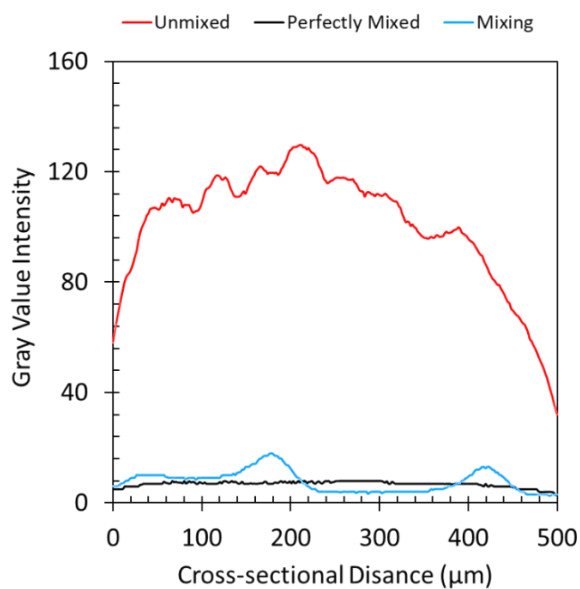


Figure S7: Fluorescence intensity profile along the microreactor cross-section for the cases of unmixed, perfectly mixed, and mixing fluorescein feeds under the conditions reported in Figure S6.

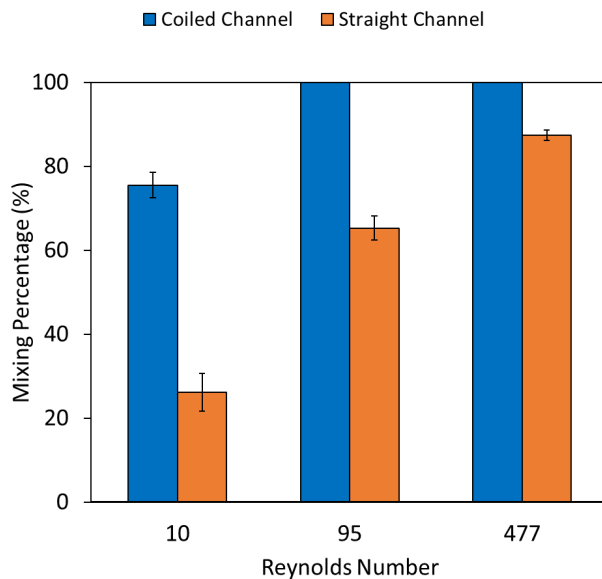


Figure S8: Comparison of the mixing degree between the coiled microchannel and a straight microchannel at a downstream distance of 6 cm from the T-micromixer, underscoring the enhancement in mixing with the coiled geometry.

PFR Model Assessment

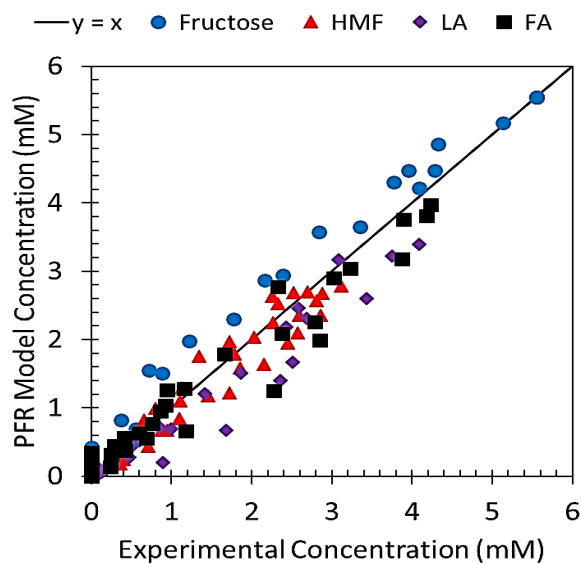


Figure S9: Parity plot of the PFR model predictions for the concentrations of fructose, HMF, LA, and FA.

Effect of Fructose Loading

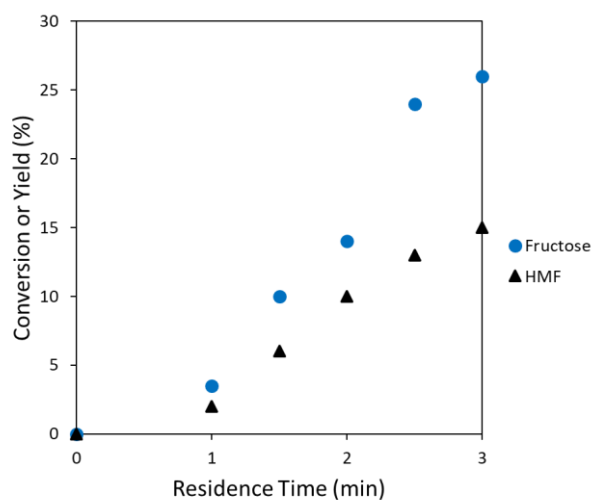


Figure S10: Time-evolution profiles of the fructose conversion and the HMF yield with no added catalyst using 5 wt% fructose at 200 °C in a single-feed reactor.

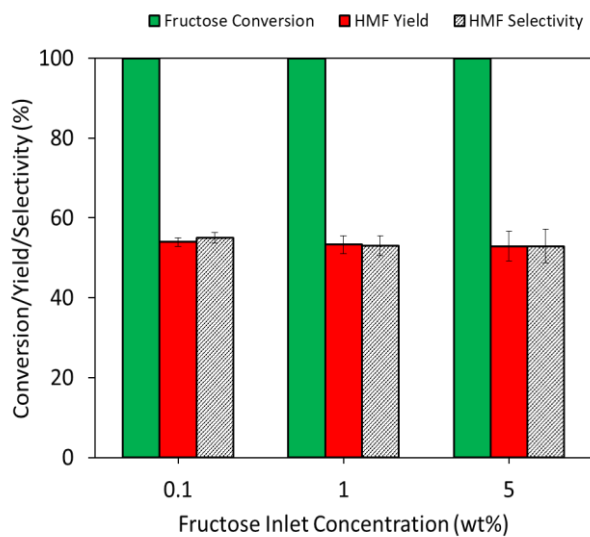


Figure S11: Experimental data on the effect of the fructose inlet concentration on the fructose conversion, HMF yield, and HMF selectivity with a 1:1 volumetric flow ratio between preheated feeds of fructose and HCl/KCl buffer solution at 200 °C and pH = 0.7.

We conducted experiments for various fructose loadings to understand the effect of fructose inlet concentration on the HMF yield and selectivity at optimal reaction conditions of high temperature and short contact times. For higher loadings, the fructose feed was preheated for 1 min to reaction temperature and mixed with the preheated acid catalyst solution at a 1:1 volumetric flow ratio. Dehydration of fructose in pure water in a single-feed microreactor at 200 °C and 5 wt% fructose, shown in Figure S10, indicates that the fructose conversion and the HMF yield are both less than 3%, suggesting no significant dehydration in the preheating section. Figure S11 shows experimental data for the fructose conversion, the HMF yield, and the HMF selectivity vs. fructose loading for high-loadings. The fructose conversion and HMF yield/selectivity remain unchanged as the fructose inlet concentration increased from 0.1 to 5 wt%. At much higher loadings, humins may form, and mitigation strategies, e.g., oxidation to generate energy or ultrasonication, will be needed for technology deployment.

Energy Dissipation Calculation

The specific energy dissipation, ε , due to the pressure drop is calculated accordingly:

$$\varepsilon = \frac{\Delta P Q_{total}}{\rho V_R} \quad (S22)$$

$$\Delta P = \frac{f L_R}{d_i} \rho \frac{U^2}{2} \quad (S23)$$

$$\tau = \frac{V_R}{Q_{total}} \quad (S24)$$

$$U = \frac{4 Q_{total}}{\pi d_i^2} \quad (S25)$$

$$V_R = \pi \frac{d_i^2}{4} L_R \quad (S26)$$

where ΔP is the pressure drop along the microreactor and V_R is the microreactor volume. Using equations (S22) through (S26):

$$\varepsilon = \frac{8 f L_R Q_{total}^2}{\pi^2 d_i^5 \tau} \quad (S27)$$

Overall Energy Efficiency Calculation

The overall energy efficiency of the process was estimated by calculating the energy efficiency of a multitubular counter-current Shell-and-Tube heat exchanger (Hex) used to heat the single-feed microreactors (made of stainless steel tubes in the Hex with $k_{channel} = 45.3 \frac{W}{m-K}$) to reaction temperature using the NTU-method^{2,3}. Scheme S3 shows a schematic of the Hex. Saturated steam at 200 °C is used as the heating fluid in the shell-side of the Hex through condensation into saturated liquid water at 200 °C. The production scale under optimal HMF productivity conditions is set at 2.5 ton/day of HMF (7 ton/day of fructose processed), which was estimated from the annual production of corn in a 600-acre farm (USDA NASS) and the highest yield of fructose obtained by enzymatic hydrolysis of corn stover^{4,5}. Thereon, the number of microreactors needed to meet the target production is calculated. The efficiency, η , is then estimated by the following equations:

$$\eta = 1 - e^{-NTU} \quad (S28)$$

$$NTU = \frac{\bar{U}_{Hex} A_{Hex}}{\dot{m}_w C_{p,w}} \quad (S29)$$

$$\frac{1}{\bar{U}_{Hex}} = \frac{d_i}{d_o h_w} + \frac{d_o}{k_{channel}} \ln\left(\frac{d_o}{d_i}\right) + \frac{1}{h_s} \quad (S30)$$

$$A_{Hex} = N_{tubes} \pi d_o L_R \quad (S31)$$

where NTU is the number of transfer units, A_{Hex} is the total heat transfer area of the Hex, \bar{U}_{Hex} is the overall heat transfer coefficient, \dot{m}_w is the mass flow rate of the aqueous fructose/water feed in the tube-side of the Hex, $C_{p,w}$ is the specific heat capacity of the aqueous fructose feed, h_w and h_s are the convective heat transfer coefficients in the tubes (water feed) and in the shell (the saturated steam), respectively, d_o and d_i are the outside and internal diameter of each reactor tube, and N_{Tubes} is the number of microreactors required. Table S3 summarizes the Hex operational conditions. Values of h_w during scale up were determined using equations (S8) and (S11) – (S17). On the other hand, h_s was estimated by using saturated steam properties and the following equations:

$$h_s = \frac{Nu_s d_{eq,shell}}{k_s} \quad (S32)$$

$$Nu_s = 0.36 Re_s^{0.55} Pr_s^{0.33} \quad (S33)$$

$$Re_s = \frac{\dot{m}_s d_{eq,shell}}{A_{c,shell} \mu_s} \quad (S34)$$

$$d_{eq,shell} = \frac{4 \left(P_t^2 - \pi \frac{d_o^2}{4} \right)}{\pi d_o} \quad (S35)$$

$$A_{c,shell} = P_t^2 - \pi \frac{d_o^2}{4} \quad (S36)$$

where Nu_s is the Nusselt number of the steam, k_s is the steam thermal conductivity, $d_{eq,shell}$ is the shell equivalent inner diameter, Re_s and Pr_s are the Reynolds and Prandtl numbers of the steam, respectively, \dot{m}_s is the mass flow rate of steam, μ_s is the dynamic viscosity of the saturated steam, $A_{c,shell}$ is the shell cross-sectional area, and P_t is the tube pitch (distance between centers of the tubes) for a square-pitch layout. The required mass flow rate of saturated steam is constant and determined from the overall energy balance between the steam feed and the aqueous fructose feed:

$$\dot{m}_s = \frac{\dot{m}_w C_{p,w} (T_s - T_{tube,in})}{\Delta H_{vap}} \quad (S37)$$

T_s is the temperature of the saturated steam in the shell, $T_{tube,in}$ is the tube inlet temperature and ΔH_{vap} is the heat of vaporization of water at 200 °C. The tube outlet temperature, $T_{tube,out}$, is then calculated:

$$T_{tube,out} = T_{tube,in} + \frac{\dot{m}_s C_{p,s}}{\dot{m}_w C_{p,w}} \eta (T_s - T_{tube,in}) \quad (S38)$$

Herein, $C_{p,s}$ is the specific heat capacity of saturated steam. During the scale-up and scale-out process, the $\frac{d_o}{d_i}$ ratio is kept constant relatively to the nominal microreactor. Furthermore, $d_{eq,shell}$ is the hydraulic diameter of the cross-section packing of the tubes (square-pitch layout) and is calculated to be 0.6 mm for the nominal microreactor. It is also kept constant during the scaling of the reactor.

Table S3. Parameters for the calculation of the energy efficiency of the Hex in order to heat (with no heat losses) 7 ton/day of 5 wt% fructose feed to 200 °C.

Feed	Flow Rate (kg/s)	Specific Heat Capacity (kJ/kg-K)	Inlet Temperature (°C)	Outlet Temperature (°C)	Pressure (bar)	Heat of Vaporization (J/kg)
Shell	0.70	3	200	200	16 ^a	1.95 x 10 ⁶
Tube	1.65	4	25	Variable	17 ^b	-

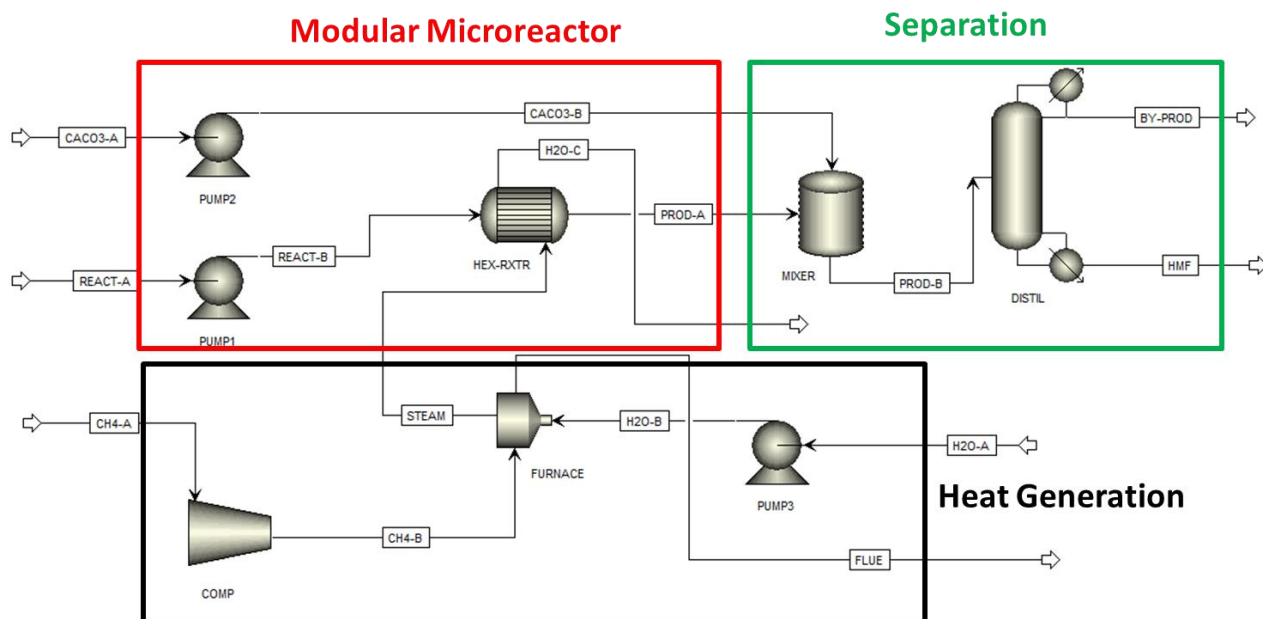
^aSaturation pressure of steam at 200 °C. ^bPressure of actual nominal microreactor to keep the reactant feed in the liquid phase.

Cost Analysis

Scheme S3 shows a process flow diagram for the hypothesized mini-plant for HMF production from fructose. The major units are the Hex containing the numbered-up reactors (HEX-RXTR) and the distillation column for HMF separation (DISTIL). The auxiliary units are the furnace (FURNACE) used to generate saturated steam at 200 °C, the mixer (MIXER) for the neutralization of the acidic product stream, pumps (PUMP1, PUMP2, and PUMP3) and the compressor (COMP) for the natural gas stream. The various streams include the reactants and catalyst (REACT-A and REACT-B), the products after reaction (PROD-A) and after neutralization (PROD-B), the calcium carbonate for the neutralization (CACO3-A and CACO3-B), the water (H2O-A, H2O-B, and H2O-C), the natural gas (CH4-A and CH4-B), the flue gas (FLUE), the by-product (BY-PROD), and the HMF (HMF). Note that the unreacted fructose in BY-PROD and HMF streams is not separated and recycled as in an actual plant and thus, our analysis would result in higher cost.

Table S4. Material and energy balances for the HMF production in the mini-plant.

Process Zone	Stream Identification	Mass Flow (lb/hr)	Pressure (bar)	Temperature (°C)	Vapor Fraction	Energy Requirement (kW)	
<i>Heat Generation</i>	CH4-A	90,252	1.0	25	1	Pumping: 70.8 Heating: 1,465	
	CH4-B	90,252	1.1	36	1		
	FLUE	90,252	1.0	152	1		
	<i>Modular Microreactor</i>	H2O-A	2,488	1.0	25	0	Pumping: 6.0
		H2O-B	2,488	16	25	0	
		STEAM	2,488	16	200	1	
<i>Separation</i>	H2O-C	2,488	16	200	0	Pumping: 14.9	
	REACT-A	13,489	1.0	25	0		
	REACT-B	13,489	17	25	0		
	PROD-A	13,489	17	200	0		
<i>Separation</i>	CACO3-A	12,787	1.0	25	0	Pumping: 13.4 Cooling: 6,993 Heating: 6,356	
	CACO3-B	12,787	17	25	0		
	PROD-B	26,276	6.9	118	0		
	BY-PROD	24,007	1.0	69	0		
	HMF	2,269	1.0	73	0		



Scheme S3: Process flow diagram for mini-plant for HMF production from fructose generated in Aspen Plus V8.6.

Table S5. Equipment sizing of the units in the mini-plant for HMF production from data calculated by individually sizing each unit, except the HEX-RXTR, in Aspen Plus V8.6.

Equipment Name	Equipment Label	Size Factor	Size	Design Temperature (°C)	Design Pressure (bar)
Feed-gas compressor	COMP	Motor power	95 Hp	36	1.1
Fired heater	FURNACE	Heat absorbed	4.4 MMBtu/hr	200	16
Multitubular dehydration reactor	HEX-RXTR	Heat transfer area	21 m ²	200	17
		Number of Tubes	1,280		
		Tube ID	0.0035 m		
		Tube length	0.5 m		
		Tube configuration	Square pitch		
Neutralization reactor	MIXER	Diameter	0.3 m	118	6.9
		x	x		
		Height	1 m		
Distillation column	DISTIL	Diameter	0.5 m	118	1.0
		x	x		
		Height	3 m		
		Number of trays	10 sieve trays		
Fructose feed pump	PUMP1	Motor power	20 Hp	25	17
Base feed pump	PUMP2	Motor power	18 Hp	25	17
Water feed pump	PUMP3	Motor power	8 Hp	25	16

The cost of the units and the total capital investment were estimated based on the method of Guthrie⁶. Key assumptions include:

- 1) The cost estimation of the equipment is based on the Chemical Engineering Plant Cost Index (CE_{index}).
- 2) The costs reported for the site and buildings are taken as 15% and 20% of the total bare-module cost of the equipment, respectively.
- 3) The cost for offsite facilities is calculated by adding 5% of the total bare-module cost to the cost for utilities (generated steam).
- 4) Land, royalties, and startup, and contingencies are estimated to be 10% and 18% of the direct permanent investment, respectively.
- 5) The working capital and labor-related operating costs are 17.6% and 4.5% of the total permanent investment, respectively

It should be noted that the relative cost analysis presented herein is only an estimate and not an extensive techno-economic analysis as our goal is to understand the effect of heat transfer on economics. The HMF minimum selling price, $\$_{HMF,min}$, is obtained as follows^{7,8}:

$$\$_{HMF,min} = \frac{\dot{M}_{Fructose}\$_{Fructose} + \dot{M}_{HCl}\$_{HCl} + \dot{M}_{KCl}\$_{KCl} + \dot{M}_{CaCO_3}\$_{CaCO_3} + \frac{E_{CH_4}\$_{CH_4}}{\eta} + C_{TCCF}}{\dot{M}_{HMF}} \quad (S39)$$

$$\dot{M}_{HMF} = \dot{M}_{Fructose} Y_{HMF}(d_i, \tau) \quad (S40)$$

where \dot{M}_i and $\$j$ are, respectively, the mass flow rate of stream i ($i = \text{Fructose, HCl, KCl, CaCO}_3, \text{HMF}$) and the price of steam j ($j = \text{Fructose, HCl, KCl, CaCO}_3, \text{CH}_4, \text{HMF}$), E_{CH_4} is the energy required to burn the shale gas, CCF is the annualization factor, C_{TCI} is the total capital investment cost, and $Y_{HMF}(d_i, \tau)$ is the HMF yield on a mass basis. Table S6 includes all the relevant economic parameters for the calculations of the total capital investment and the HMF minimum selling price. Given that the single-feed tubes are heated by the Hex, the reactor is no longer isothermal, and the rate of heat transfer depends on d_i since both \bar{U}_{Hex} and A_{Hex} change with d_i during the scale-up and scale-out. Thereon, for the cost analysis, the reactor is modeled as a non-isothermal PFR by simultaneously solving for the temperature profile along the reactor in addition to the species mass balance in equations (1) through (6):

$$\frac{dT_{rxn}}{d\tau} = \frac{\bar{U}_{Hex} A_{Hex} (T_s - T_{tube,in})}{\rho_w C_{p,w} V_R} \quad (S41)$$

where T_{rxn} is the reaction temperature and ρ_w is the density of the aqueous fructose-feed. In solving for the temperature profile with residence time, we assume that both the pressure drop and the heat of reaction are negligible throughout the reactor. Moreover, as d_i increases during the scale-up and scale-out process, the product $\bar{U}_{Hex} A_{Hex}$ decreases, underscoring poor heat transfer with temperatures lower than the optimal temperature of 200 °C and lower yields. Thereon, a lower production rate of HMF is obtained, increasing its minimum selling price, according to equation (S39). Furthermore, optimal scale-up conditions are employed for the largest scaled-up microreactor diameter and the number of reactors to create a module (scale out) is estimated to produce HMF at the selling price at 5 wt% fructose loading. Figure S12 shows the breakdown of the total capital investment for farm-scale HMF production. The low capital investment cost of \$2.3 MM underscores that modular manufacturing for HMF production at the farm-scale is economically feasible. Moreover, the largest cost fraction (18% of the total capital investment) stems from supplying steam (heat generation zone). Figure S13 shows that the HMF minimum selling price is mainly driven by the price of the fructose feedstock, consistent with the works by Tsapatsis and co-workers^{7,8} and Dumesic and co-workers⁹. However, the total capital investment is also a significant contributor to this while the capital cost has been shown to be a small fraction of the price in studies using conventional reactors with longer reaction times and higher HMF yields in multi-solvent systems⁹. Consequently, adopting more energy efficient heating methods with fast heating rates and developing technologies producing a cheaper fructose feedstock from renewable biomass are necessary to further reduce both the capital cost and the HMF minimum selling price to possibly envision an economically sustainable HMF production.

Table S6. Values of the economic parameters used in the cost analysis.

Economic Parameter	Value	Units
CE_{index} (base cost)	394	-
CE_{index} (2018)	603	-
CCF	0.33	-
$\$Fructose$	0.20 ^a	\$/lb
$\$HCl$	0.02 ^b	\$/lb
$\$KCl$	0.10 ^b	\$/lb
$\$CaCO_3$	0.13 ^b	\$/lb
$\$CH_4$	3.80 ^c	\$/MMBtu

^aValues taken as the average of previously published studies^{8,10}. ^bValues taken from ICIS. ^cValues taken from FORBES.

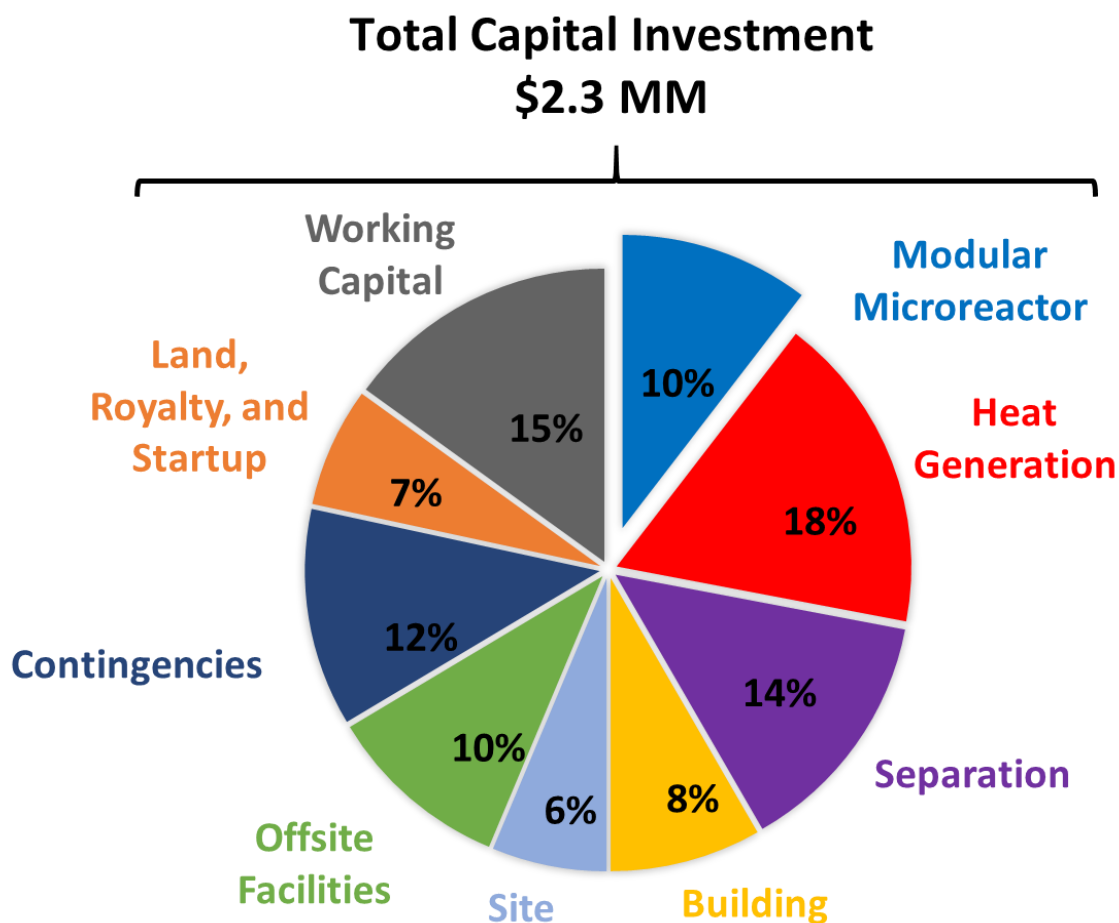


Figure S12: Breakdown of the total capital investment for the farm-scale production of HMF (2.5 ton/day) under optimal scale-up conditions (reactor ID = 3.5 mm) for a 5 wt% fructose loading.

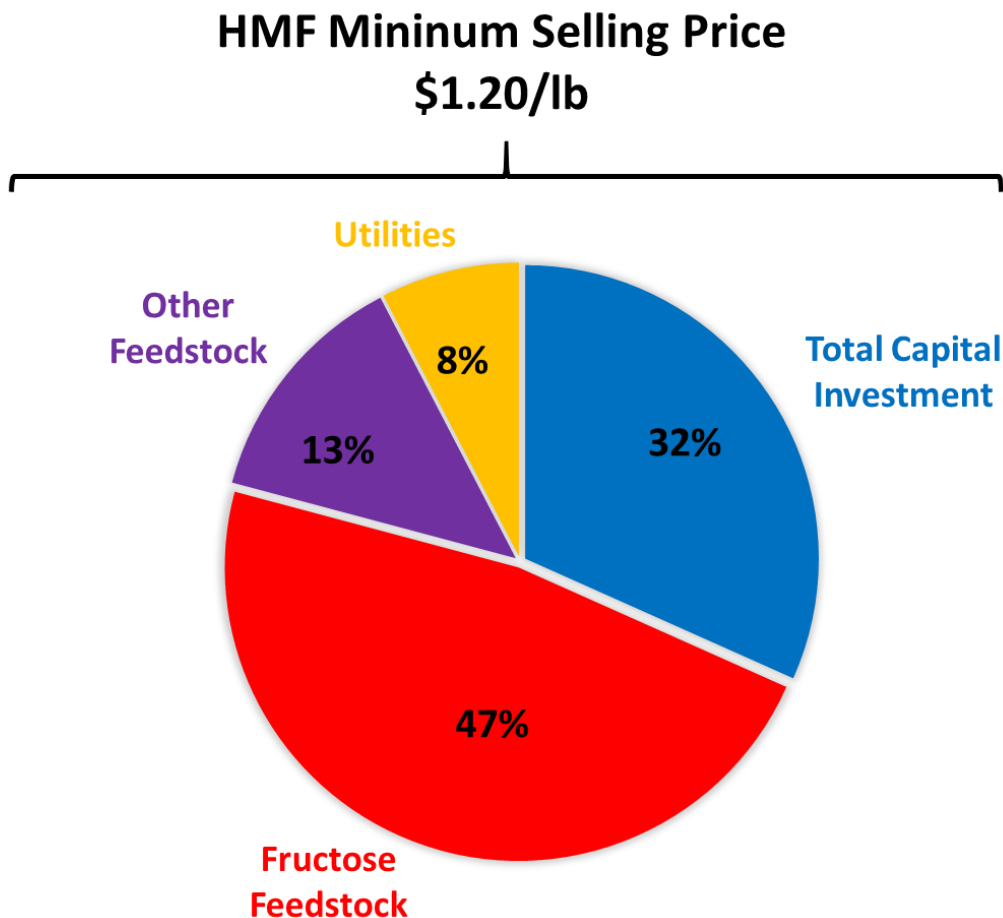


Figure S13: Relative contribution of the components of the HMF minimum selling price for farm-scale production (2.5 ton/day) under optimal scale-up conditions (reactor ID = 3.5 mm) for a 5 wt% fructose loading.

We also investigated the effect of a larger plant size (30 HMF ton/day) on the cost of HMF production via the microprocess. We compared our results to the recent study by Motagamwala *et al.*⁹ using an acetone/water solvent with ~90% HMF yield in a conventional continuous flow reactor. The data in Table S7 demonstrate that, with a 12-fold increase in plant size, the microprocess is more cost-competitive with 18% and 27% lower fixed operating and capital costs, respectively, when compared to the conventional process. Nonetheless, the microprocess incurs a higher variable operating cost due to the high HCl concentrations needed to achieve the short reaction times and the high CaCO₃ concentrations needed to neutralize the product mixture. Although the HMF minimum selling price is reduced at the larger plant size (the feed flow rates and the energy requirement to burn the shale gas increase 12-fold while the total capital investment increases 5-fold in the larger plant in equation (S39)), the conventional reactor process has a lower selling price due to the higher HMF yields obtained with the water/acetone system.

Table S7. Effect of plant sizing on cost of HMF production.

	Plant Size (HMF ton/day)	Total Capital Investment (MMS)	Variable Operating Costs (MMS/yr)	Fixed Operating Costs (MMS/yr)	HMF Minimum Selling Price (\$/lb)
This work	2.5	2.3	1.6	0.36	1.20
This work	30	11.9	19.9	0.82	0.99
Motagamwala <i>et al.</i>⁹	30	16.2	16.5	1.0	0.78

Table S8. Equations, symbols, and units included in the supplementary information.

Symbol	Variable Name	Units
$\$_{CH_4}$	Market price of natural gas	\$/MMBtu
$\$_{CaCO_3}$	Market price of CaCO ₃	\$/lb
$\$_{Fructose}$	Market price of fructose	\$/lb
$\$_{HCl}$	Market price of HCl	\$/lb
$\$_{HMF,min}$	Minimum selling price of HMF	\$/lb
$\$_{KCl}$	Market price of KCl	\$/lb
\dot{M}_{CaCO_3}	Mass flow rate of CaCO ₃	lb/yr
$\dot{M}_{Fructose}$	Mass flow rate of Fructose	lb/yr
\dot{M}_{HCl}	Mass flow rate of HCl	lb/yr
\dot{M}_{HMF}	Mass flow rate of HMF	lb/yr
\dot{M}_{KCl}	Mass flow rate of KCl	lb/yr
\bar{U}_{Hex}	Overall heat transfer coefficient of the heat exchanger	W/m ² -K
\dot{m}_1	Mass flow rate of feed 2	kg/s
\dot{m}_2	Mass flow rate of feed 3	kg/s
\dot{m}_{in}	Mass flow rate of the reactor inlet feed	kg/s

\dot{m}_s	Mass flow rate of saturated steam in the heat exchanger	kg/s
\dot{m}_w	Mass flow rate of water in the heat exchanger	kg/s
ΔH_{vap}	Heat of vaporization of water at 200 °C	J/kg
h_{air}	Convective heat transfer coefficient of air in the furnace	W/m ² -K
h_s	Convective heat transfer coefficient of saturated steam in heat exchanger	W/m ² -K
h_w	Convective heat transfer coefficient of water in heat exchanger	W/m ² -K
h_{water}	Convective heat transfer coefficient of water in the microchannel	W/m ² -K
A_{Hex}	Total surface area for heat transfer in the heat exchanger	m ²
$A_{c,shell}$	Cross-sectional area of the shell-side of the heat exchanger	m ²
A_c	Cross-sectional area of the microchannel	m ²
$C_{p,w}$	Specific heat capacity of water in the heat exchanger	J/kg-K
C_p	Specific heat capacity of water	J/kg-K
E_{CH4}	Energy required for the combustion of natural gas	MMBtu
I_i	Dye intensity at pixel i during mixing in the microchannel	pixel
$I_i^{Perf,mix}$	Dye intensity at pixel i of perfectly mixed feeds in the microchannel	pixel
$I_i^{Perf,mix}$	Dye intensity at pixel i of unmixed dye solution in the microchannel	pixel
L_H	Hydrodynamic entrance length in the microchannel	m
L_R	Microreactor length	m

L_T	Thermal entrance length in the microchannel	m
L_{mixing}	Mixing length along the microchannel	m
N_{tubes}	Number of tubes in the heat exchanger	-
Nu_s	Nusselt number of saturated steam in the heat exchanger	-
Pr_s	Prandtl number of saturated steam at 200 °C	-
P_t	Tube pitch	m
Q_1	Volumetric flow rate of feed 1	m ³ /s
Q_2	Volumetric flow rate of feed 2	m ³ /s
Q_{total}	Total volumetric flow rate in the microchannel	m ³ /s
$R_{cond,channel}$	Heat transfer resistance by conduction through the microchannel wall	m ² -K/W
$R_{conv,air}$	Heat transfer resistance by convection of hot air in the furnace	m ² -K/W
$R_{conv,water}$	Heat transfer resistance by convection of water flowing through the microchannel	m ² -K/W
Re_s	Reynolds number of saturated steam in the heat exchanger	
T_1	Temperature of feed 1	K
T_2	Temperature of feed 2	K
T_f	Furnace temperature	K
T_{in}	Temperature of the reactor inlet feed	K
$T_{m,in}$	Average temperature of water at the inlet of the microchannel	K
$T_{m,out}$	Average temperature of water at the outlet of the microchannel	K

T_m	Average temperature of water in the microchannel	K
T_{ref}	Reference temperature	K
T_{rxn}	Reaction temperature in the tubes of the heat exchanger	K
T_s	Saturated steam temperature in the heat exchanger	K
$T_{tube,in}$	Tube inlet temperature in the heat exchanger	K
$T_{tube,out}$	Tube outlet temperature in the heat exchanger	K
\bar{U}	Overall heat transfer coefficient of the microchannel	W/m ² -K
V_R	Microreactor volume	m ³
$Y_{HMF}(d_i, \tau)$	Yield of HMF in mass fraction	-
$d_{eq,shell}$	Equivalent diameter of the shell in the heat exchanger	m
d_i	Microchannel inner diameter	m
d_o	Microchannel outer diameter	m
$k_{channel}$	Thermal conductivity of the microchannel wall	W/m-K
k_s	Thermal conductivity of saturated steam at 200 °C	W/m-K
t_{mixing}	Mixing time in the microchannel	s
x_1	Coefficient 1 in Nusselt number calculations	-
x_2	Coefficient 2 in Nusselt number calculations	-
x_3	Coefficient 3 in Nusselt number calculations	-
x_4	Coefficient 4 in Nusselt number calculations	-

μ_s	Dynamic viscosity of saturated steam at 200 °C	Pa-s
σ_n^2	Noise in intensity of the dye in the microchannel	pixel ²
ΔP	Pressure drop in the microchannel	Pa
A	Surface area for heat transfer of the microreactor	m ²
De	Dean number of water in the microchannel	-
N	Number of pixels	-
NTU	Number of transfer units	-
Nu	Nusselt number of water in the microchannel	-
<i>Percent Mixing</i>	Percent mixing in the microchannel	%
Pr	Prandtl number of water in the microchannel	-
R	Volumetric flow rate ratio between feed 2 and feed 1	-
Re	Reynolds number of water in the microchannel	-
U	Linear speed of water in the microchannel	m/s
f	Darcy friction factor	-
q	Heating rate of the furnace	W
α	Thermal diffusivity of water	m ² /s
ε	Specific energy dissipation due to pressure drop	W/kg
η	Heat exchanger thermal efficiency	-
ν	Kinematic viscosity of water	m ² /s
ρ	Density of water	kg/m ³

Supplementary Information References

1. W. M. Rohsenow, J. P. Hartnett and E. N. Ganic, *Handbook of heat transfer fundamentals*, McGraw-Hill, New York, 1985.
2. R. K. Shah and D. P. Sekulic, Fundamentals of heat exchanger design, <http://dx.doi.org/10.1002/9780470172605>.
3. H. S. Lee, *Thermal design : heat sinks, thermoelectrics, heat pipes, compact heat exchangers, and solar cells*, Wiley, Hoboken, NJ, 2010.
4. H. Li, S. Yang, S. Saravanamurugan and A. Riisager, *Acs Catalysis*, 2017, **7**, 3010-3029.
5. M. Galbe and G. Zacchi, in *Biofuels*, ed. L. Olsson, 2007, vol. 108, pp. 41-65.
6. W. D. Seider, *Product and process design principles : synthesis, analysis, and evaluation*, John Wiley, Hoboken, NJ, 2009.
7. A. I. Torres, M. Tsapatsis and P. Daoutidis, *Computers & Chemical Engineering*, 2012, **42**, 130-137.
8. A. I. Torres, P. Daoutidis and M. Tsapatsis, *Energy & Environmental Science*, 2010, **3**, 1560-1572.
9. A. H. Motagamwala, K. Huang, C. T. Maravelias and J. A. Dumesic, *Energy & Environmental Science*, 2019.
10. F. K. Kazi, A. D. Patel, J. C. Serrano-Ruiz, J. A. Dumesic and R. P. Anex, *Chemical Engineering Journal*, 2011, **169**, 329-338.